

Cluster-surface and cluster-cluster interactions: ab initio calculations and modelling of asymptotic van der Waals forces

Silvana Botti,^{1,2,3,4,*} Alberto Castro,^{5,4} Xavier Andrade,^{6,4} Angel Rubio,^{6,4} and Miguel A. L. Marques^{3,2,4}

¹*Laboratoire des Solides Irradiés, CNRS-CEA-École Polytechnique, Palaiseau, France*

²*Centro de Física Computacional, Departamento de Física, Universidade de Coimbra, Coimbra, Portugal*

³*LPMCN, Université Claude Bernard Lyon I and CNRS UMR 5586, 69622 Villeurbanne, France*

⁴*European Theoretical Spectroscopy Facility*

⁵*Institut für Theoretische Physik, Fachbereich Physik der Freie Universität Berlin, Arnimallee 14, D-14195 Berlin, Germany*

⁶*European Theoretical Spectroscopy Facility, Departamento de Física de Materiales, Universidad del País Vasco, Centro Mixto CSIC-UPV, and Donostia International Physics Center (DIPC), Av. Tolosa 72, E-20018 San Sebastián, Spain*

(Dated: November 27, 2021)

We present fully ab-initio calculations of van der Waals coefficients for two different situations: i) the interaction between hydrogenated silicon clusters; and ii) the interactions between these nanostructures and a non metallic surface (a silicon or a silicon carbide surface). The methods used are very efficient, and allow the calculation of systems containing hundreds of atoms. The results obtained are further analyzed and understood with the help of simple models. These models can be of interest for molecular dynamics simulations of silicon nanostructures on surfaces, where they can give a very fast yet sufficiently accurate determination of the van der Waals interaction at large separations.

I. INTRODUCTION

The van der Waals interaction is a common presence in the worlds of Physics, Chemistry, and Biology.¹ Studied for more than a century,² it is a dispersive force that, being weak at short distances, becomes the dominant attraction between neutral bodies at large separations. It results from the non-zero multipole-multipole attraction stemming from transient quantum fluctuations. It is the interplay between the electrostatic and dispersive interactions that determines many interesting phenomena in Nature, even in the macroscopic world. For example, it is van der Waals interactions that are responsible for the remarkable ability of geckos to hold to surfaces.³ A significant example of application of van der Waals interactions comes from some operating modes of atomic force microscopes.⁴

However, the realm of van der Waals forces, being quantum in nature, is the world of atoms and molecules — the nano world. In fact, these forces determine the structure of DNA molecules, the folding and dynamics of proteins, the adsorption of atoms, molecules or nanostructures on surfaces, etc. Moreover, the van der Waals atom-surface interaction has also been recently studied due to their influence on the quantum reflection of ultracold atoms on surfaces.⁵ In fact, the upsurge of interest on Bose-Einstein condensation of ultracold atoms confined in magnetic traps⁶ near a surface should fuel research on atom-surface dispersion interactions, since they are key factors for the stability of the condensate. They are also key ingredients in the building and functioning of many of the systems relevant for the emerging fields of nanotechnology and biotechnology. For example, their effect was shown to have a profound influence on the oscillatory behavior of microstructures when surfaces are in close proximity (100 nm).⁷

In this context, the purpose of this Article is to present fully ab-initio calculations of the van der Waals coefficients for the interaction between nanostructures (silicon clusters, in particular) and between these nanostructures and surfaces. These results are then used to formulate simple models that describe with enough precision the van der Waals interactions. The models are important, as they can be the starting point for, e.g., molecular dynamics simulations of the behavior of silicon nanostructures at surfaces. We will be looking at large separations, when the overlap between the electronic clouds is negligible. At shorter distances, the situation is considerably more complicated and no satisfying description has emerged yet.

Typically, van der Waals interactions decay with an inverse power of the distance between the two bodies under consideration; The exponent depends on their their dimensionality or their metallic character.⁸ We are interested in two specific cases:

A) *The interaction between two finite nanostructures*, namely atomic clusters of silicon, saturated with hydrogen. We restrict ourselves to the more interesting non-retarded regime, i.e. when the time that it takes for the photons to travel between the two molecules is negligible. In this case, the van der Waals interaction energy has an expansion with respect to the inverse of the intermolecular distance ($1/R$) of the form

$$\Delta E(R) = - \sum_{n=6}^{\infty} \frac{C_n}{R^n} \quad (1)$$

in terms of the Hamaker constants C_n .^{1,9} The first term C_6 for a pair of molecules A and B , averaged over all possible orientations, can be obtained through the relation (atomic units will be used hereafter):

$$C_6^{AB} = \frac{3}{\pi} \int_0^{\infty} du \alpha^{(A)}(iu) \alpha^{(B)}(iu), \quad (2)$$

where $\alpha^{(X)}(iu)$ is the average of the dipole polarizability tensor of molecule X , $\alpha^{(X)}$, evaluated at the imaginary frequency iu :

$$\alpha^{(X)}(iu) = \frac{1}{3} \text{Tr}[\alpha^{(X)}(iu)]. \quad (3)$$

The higher order terms in the expansion (1) can in a similar way be written in terms of higher order polarizability tensors. For example, the C_8 coefficient will depend on the dipole-quadrupole dynamic polarizability (see, e.g., Ref. 10). In this article we will focus on the leading term of the expansion, i.e. the Hamaker constant C_6 .

B) *The interaction between a nanostructure and a surface.* Here we will focus on silicon and silicon carbide surfaces. In this case, the leading term of the expansion of the van der Waals energy as a function of the distance Z between the cluster and the surface is proportional to Z^{-3} . This fact was first established by Lennard-Jones,¹¹ who used a model with a perfectly reflecting metal. The theory was later developed by Casimir and Polder,¹² and by Lifschitz.¹³ For a wide range of particle-substrate distances (from approximately 1 nm to even 10^3 nm), the interaction energy is given by:

$$\Delta E(Z) = -\frac{C_3}{(Z - Z_0)^3}, \quad (4)$$

where Z_0 is a ‘‘reference plane’’, and C_3 is the Lifshitz coefficient. This coefficient can be calculated from the dynamical polarizability of the cluster, $\alpha(iu)$, and the macroscopic dielectric function of the bulk material, $\epsilon_M(iu)$, both evaluated at imaginary frequencies, iu :

$$C_3 = \frac{1}{4\pi} \int_0^\infty du \alpha(iu) \frac{\epsilon_M(iu) - 1}{\epsilon_M(iu) + 1}. \quad (5)$$

Note that C_3 is expressed only in terms of quantities calculated for the bulk crystal. This expression is a general result, also valid for metallic surfaces. The quantity that depends on the characteristics of the surface is the position of the reference plane Z_0 . However, for semi-conducting surfaces, it can be shown¹⁴ that, in absence of local field effects, Z_0 is equal to $a/2$, where a is the interplanar distance. Moreover, it is known that even relatively large local field corrections give rise to rather small shifts of the reference plane.¹⁴ Note, however, the position of the reference plane Z_0 is a more delicate issue in the case of a metal, as positioning the reference plane at a distance of $a/2$ from the surface can lead to significant errors in the interaction energy (i.e. about 30% for a noble metal surface).¹⁴ Further analysis to determine the dependence of van der Waals interactions on the surface response are under progress.

It is interesting to remark that it took a long time to verify experimentally the predicted Z^{-3} dependence. Although this term dominates a very wide distance region, in the short distance regime it is only a tail of the particle potential whose minimum determines the adsorption.

The first precise measurement of the van der Waals coupling between an atom and a surface was reported in Ref. 15; later on some more experiments have followed.¹⁶ The experimental difficulties are, in fact, in pair with the theoretical ones, since fully ab initio calculations are also challenging. Most of the calculations reported in the literature^{17,18} are generally limited to atoms or very small molecules, and the bulk detailed microscopic structure is replaced by some model (e.g., the stabilized jellium model for metals). An interesting approach consists in modelling the molecular polarizability using the form of the long-wavelength density response of a homogeneous electron gas. The van der Waals interaction is thus efficiently described by the ground-state electron densities of the interacting species, obtaining C_6 coefficients that on average deviate 9% from those obtained by TDDFT calculations.¹⁹ All approximations were justified by the authors by the difficulty of treating medium size molecules within a full ab initio TDDFT approach.

It is the purpose of our work to demonstrate that current ab initio techniques permit the calculation of the van der Waals coefficients for large nanostructures interacting with realistically described surfaces. The rest of this Article is structured as follows: In Section II we review the methods used to evaluate the dynamical polarizabilities and the dielectric functions at imaginary frequency; in the following section we present the results of our ab initio calculations, that are then further analyzed in Section IV using some simple models. Finally, we draw some conclusions in Section V.

II. METHODS

The main ingredients to evaluate the van der Waals coefficients are therefore the electronic polarizability α of the cluster and the dielectric constant of the bulk material ϵ , both evaluated at imaginary frequencies. The computational methods and the problems involved in the calculation of these two quantities are quite different, so we will discuss them separately.

A. Dynamical polarizabilities

In principle, one can obtain the dynamical polarizabilities by making use of any quantum-chemistry theory capable of handling time-dependent perturbations. As the nanostructures we are interested in can be fairly large, we choose the time-dependent (TD) extension of density functional theory (DFT), since this approach provides an excellent compromise between accuracy and feasibility. During the past decade, TDDFT²⁰ has become one of the most important tools to study electronic excitations of molecular systems, especially for medium and large systems where it is often the only feasible alternative.

Several different numerical approaches can be found in the literature to calculate α at imaginary frequencies

within TDDFT. For example, linear response theory can be employed to calculate the density-density response function χ , from which α directly follows:

$$\alpha_{ij}(\omega) = \int d^3r \int d^3r' r_i \chi(\mathbf{r}, \mathbf{r}', \omega) r_j. \quad (6)$$

This approach is quite common and has been used for the calculation of the C_6 coefficients of molecules and clusters.²¹ Alternatively, one can work in real time: By propagating the Kohn-Sham equations in real time, it is immediate to obtain $\alpha(t)$. A Laplace transformation of this quantity yields $\alpha(iu)$ and therefore the Hamaker constant C_6 . Recently, some of us have shown²² how this procedure can effectively provide C_6 coefficients of large molecules. A slightly different approach is the polarization propagation technique, whose extension to imaginary frequencies has been used to compute C_6 coefficients.²³ For very large systems, Banerjee and Harbola have proposed the use of orbital free TDDFT, providing satisfactory results for large sodium clusters.²⁴

In this article, we use an alternative scheme based on the solution of a Sternheimer equation.²⁵ It avoids the use of empty states, therefore providing a quite good scaling (N^2) with the number of atoms. The real-time propagation technique mentioned above has a similar scaling, but we find the prefactor of the Sternheimer approach to be smaller. This method has already been used for the calculation of many response properties, like atomic vibrations, electron-phonon coupling, magnetic response, etc.²⁶ In the domain of optical response, it has been mainly used for static response, although a few calculations at finite (real) frequency have appeared.²⁷

We have implemented the Sternheimer equation at imaginary frequency in the real-space code `octopus`.²⁸ The details are explained in Ref. 29 – although in that case the equation is solved for real frequencies. A generalization to imaginary frequencies is straightforward. The efficiency of the Sternheimer approach is illustrated by the size of the clusters studied in this Article: up to $\text{Si}_{172}\text{H}_{120}$, i.e., ~ 300 atoms, computed with relatively modest computer systems. Note that, for these systems, the time required for the evaluation of the van der Waals coefficients is of the same order as the time required for the ground-state calculation.

B. Dielectric constant

The electronic band structure of bulk semiconductors and insulators, which is the starting point to obtain the dielectric functions, can nowadays be accurately computed with ab initio methods.³⁰ Much work has been done in the past years to determine which approximations allow a proper description of electron-electron and electron-hole interactions, which is essential to obtain optical functions (at real frequencies) in agreement with experimental data.³¹

The inverse microscopic dielectric function ϵ^{-1} of a periodic system is related to the response function χ :

$$\epsilon^{-1}(\mathbf{q}, \mathbf{G}, \mathbf{G}', \omega) = \delta_{\mathbf{G}, \mathbf{G}'} + v(\mathbf{q}, \mathbf{G}) \chi(\mathbf{q}, \mathbf{G}, \mathbf{G}', \omega), \quad (7)$$

where \mathbf{q} is a vector in the Brillouin zone, \mathbf{G} is a reciprocal lattice vector, and v is the bare Coulomb interaction. The response function χ obeys the matrix equation

$$\chi = \chi_0 + \chi_0 (v + f_{xc}) \chi, \quad (8)$$

χ_0 being the independent-particle Kohn-Sham response function, and f_{xc} the so-called xc kernel. The macroscopic dielectric function ϵ_M can be readily obtained from the microscopic ϵ :

$$\epsilon_M(\omega) = \lim_{\mathbf{q} \rightarrow 0} \frac{1}{\epsilon^{-1}(\mathbf{q}, \mathbf{G} = 0, \mathbf{G}' = 0, \omega)}. \quad (9)$$

The simplest approximation that yields the dielectric function consists in applying Fermi's golden rule. In this approximation, the optical spectrum is calculated as a sum of independent transitions between Kohn-Sham (KS) or quasiparticle states. This poor man's approach is known to exhibit severe shortcomings compared to experiments.³² The next step is the so-called random phase approximation (RPA), that includes the effects due to the variation of the Hartree potential upon excitation, while f_{xc} is set to zero. Unfortunately, the RPA does not lead to any significant improvement for most solids, especially if there are no particularly pronounced polarizable inhomogeneities in the charge density. Replacing the KS energies with the quasiparticle energies does not solve the problem: the peak positions are usually over-corrected and the oscillator strength is not modified.

It is the neglect of variations of the xc potential, which include the effect of the electron-hole Coulomb interaction, that is responsible for an overall disagreement in the absorption strength – in particular for the failure to reproduce continuum and bound excitons. Unfortunately, the adiabatic local density approximation (TDLDA) for the xc-kernel in the case of solids is not sufficient to yield good dielectric functions. The reason for this failure can be traced back to the short-range nature of the TDLDA f_{xc} , while the “exact” f_{xc} is expected to be long-ranged,³¹ decaying in momentum space as $1/q^2$.

A class of kernels that was shown to yield good results is those derived from the Bethe-Salpeter equation (BSE),^{31,33,34} used together with the quasiparticle band-structure. A parameter-free expression, the “nanoquanta kernel”, was obtained in several different ways (for a detailed discussion we refer the reader to Ref. 34, and references therein). Although involving a potentially reduced computational effort with respect to the BSE, these calculations are still significantly more cumbersome than those within the RPA or the TDLDA. To keep the computational cost as low as possible, in many cases it is enough to use simplified versions of this kernel. It was shown that the nanoquanta kernel has the asymptotic

form of a long-range contribution (LRC)^{35,36}

$$f_{xc}^{\text{static}}(\mathbf{q}) = -\frac{\alpha^{\text{static}}}{q^2}, \quad (10)$$

where α^{static} is a material dependent parameter, that can be related to the dielectric constant. This long-range contribution alone is sufficient to simulate the strong continuum exciton effect in the absorption spectrum and in the refraction index of several simple semiconductors, like bulk silicon or GaAs, provided that quasiparticle energies are used as a starting point. A dynamical extension of this LRC model³⁷ of the form

$$f_{xc}^{\text{dyn}}(\mathbf{q}) = -\frac{\alpha + \beta\omega^2}{q^2} \quad (11)$$

leads to remarkable improvements for optical spectra of large gap systems with respect to calculations where the kernel is imposed to be static. Moreover, the dynamical approach was proved to be valid also for energies in the range of plasmons and for the determination of dielectric constants. Note that the parameters of both the static and the dynamical model can be related to physical quantities, like the experimental dielectric constant and the plasmon frequency.

In this work, we calculated the dielectric functions at imaginary frequency using the computer code DP,³⁸ an ab initio linear response, plane wave, TDDFT code. Despite the enormous amount of studies concerning the accuracy of different approximations for the xc kernel for solids, it is not a priori clear which approximation is more suitable when one wants to work at imaginary frequencies. In order to clarify this aspect, we tested several approximations for the xc kernel.

III. CALCULATIONS

A. van der Waals interactions between silicon clusters

We start our discussion by the calculation of C_6 between the silicon clusters. The clusters were cut from bulk silicon, and then saturated with hydrogens along the tetrahedral direction of the surface atoms. The geometries were optimized with the computer code siesta,³⁹ employing norm-conserving pseudopotentials, a double ζ with polarization basis set, and the PBE parametrization⁴⁰ for the xc potential.

From the optimized geometries, we then obtained the electric polarizability within TDDFT using the Sternheimer equation, as implemented in the computer code octopus.²⁸ The electron-ion interaction was described through norm-conserving pseudopotentials⁴¹ and the local density approximation (LDA)⁴² was employed in the adiabatic approximation for the xc potential. It is known that the LDA provides reliable results for semiconducting clusters⁴³; Furthermore, from previous experience with

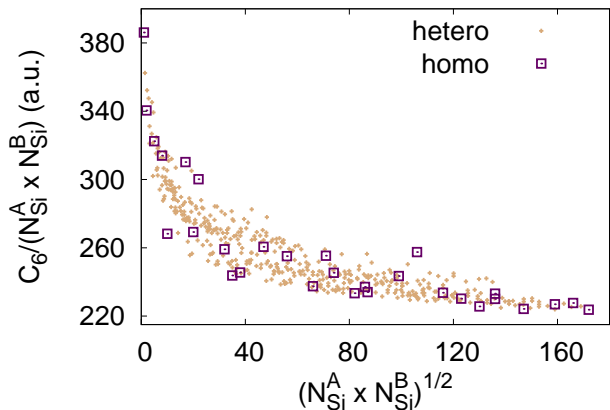


FIG. 1: (Color online) C_6^{AB} Hamaker constants as a function of the square root of the product of silicon atoms in cluster A and B. As C_6^{AB} scales basically with the product between the number of (silicon) atoms in A and B, we plot the Hamaker constants divided by this number. Values of C_6^{AB} when A and B are the same cluster are plotted as red (dark gray) squares, otherwise they are plotted as orange (light gray) dots.

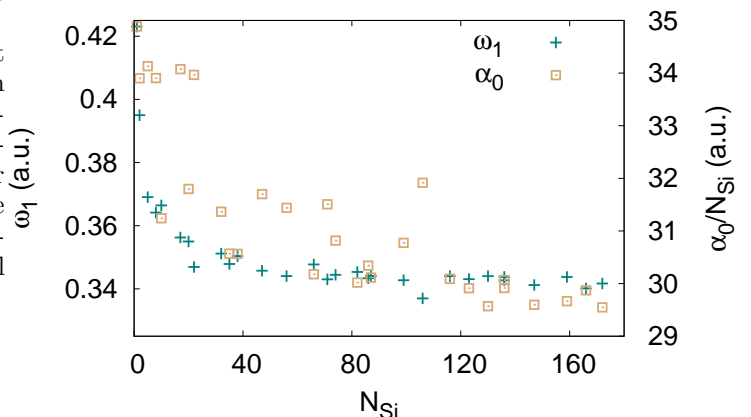


FIG. 2: (Color online) London effective frequency ω_1 – blue (dark gray) crosses, and static polarizabilities per atom – red (light gray) squares, for the silicon clusters under study, as a function of the number of silicon atoms.

optical spectra calculations,⁴⁴ we know that these results will not change significantly with the use of the more sophisticated GGAs. The equations, in this code, are represented in a real-space regular grid, whose spacing is chosen to be 0.275 Å. The simulation box is constructed by joining spheres of radius 4.5 Å, centered around each atom. The integrals in Eqs. (2) and (5) were performed with a Gauss-Legendre quadrature using 6 frequency values. With these parameters, we estimate the accuracy of our numerical calculations to better than 5%.

In Fig. 1 we show our results for the C_6 Hamaker constant between silicon clusters. As the value of C_6 scales with the product of the atoms in the cluster A (N_{Si}^A) and

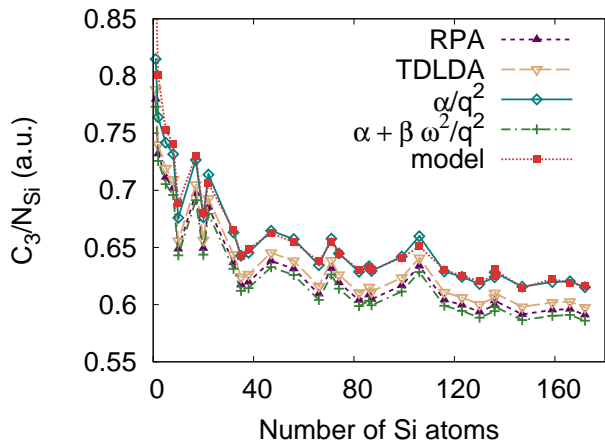


FIG. 3: (Color online) Van der Waals C_3 coefficients between silicon nanoclusters and a silicon surface. The C_3 coefficients were divided by the number of silicon atoms in the cluster. The different curves were calculated using different approximations for the dielectric constant of the bulk crystal at imaginary frequencies (see the text for details).

in cluster B (N_{Si}^B), we divided the Hamaker constant by $N_{Si}^A N_{Si}^B$ to eliminate this dependence. We show both constants between two identical clusters (homo-molecular – as red (dark gray) squares, also presented in Table I) and between different clusters (hetero-molecular – orange (light gray) dots). We see that the largest C_6 per atom squared comes from the interaction between two SiH_4 clusters, and then the values decrease rapidly until slightly above 220 a.u., where it saturates. The few clusters that fall far from the line are the most asymmetric, for which a description in terms of the average of the dipole polarizability tensor is not necessarily as good.

The polarizability at imaginary frequencies can be modelled in the London approximation by introducing two adjustable parameters: the static polarizability $\alpha(0)$ and one effective frequency ω_1 :

$$\alpha(iu) = \frac{\alpha(0)}{1 + (u/\omega_1)^2}. \quad (12)$$

If we insert (12) in (2) we obtain a simplified expression for the homo-molecular Hamaker constant in terms of these parameters:

$$C_6 = \frac{3\omega_1}{4} \alpha^2(0). \quad (13)$$

As we have calculated both C_6 and $\alpha(0)$ within TDLDA, it is easy to extract ω_1 from Eq. (13). The resulting effective frequencies are plotted in Fig. 2, together with the calculated static polarizabilities per number of Si atoms. We can observe that ω_1 decreases with the number of Si atoms, but the dependence on the size of the cluster is rather weak, except for the singular case of the smallest aggregates.

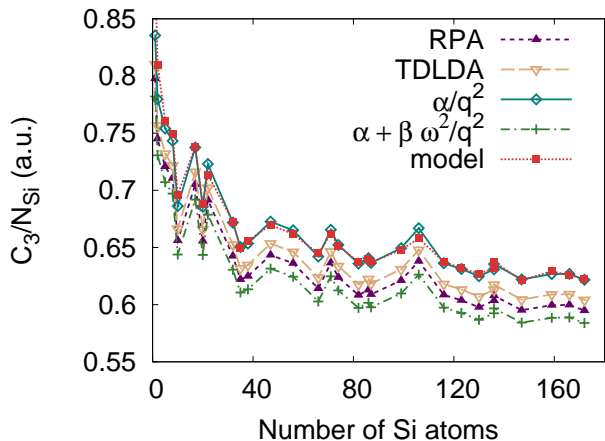


FIG. 4: (Color online) Van der Waals C_3 coefficient between silicon nanoclusters and a silicon carbide surface. The meaning of the curves is as in Fig. 3.

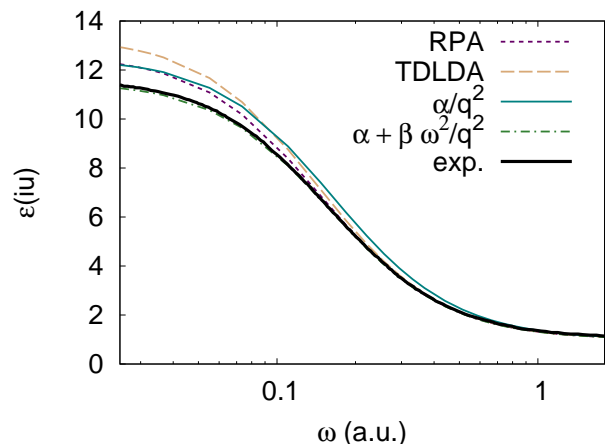


FIG. 5: (Color online) Dielectric function of Si along the imaginary axis as a function of the frequency in a logarithmic scale. Results obtained with different approximations for the xc kernel are compared to the curve extracted from experimental data by using Eq. (14.)

B. van der Waals interactions between silicon clusters and dielectric surfaces

Next, we consider the case of a silicon cluster in proximity of a surface of Si or SiC in the zincblende phase. In this case we want to calculate C_3 coefficients, that are determined both by the dynamical polarizability of the cluster and the dielectric function of the bulk crystal.

The ground state calculations for the bulk crystals were performed using the plane-wave code ABINIT⁴⁵ with norm-conserving Hamann pseudopotentials⁴⁶ for Si and C. We used a cutoff energy for the plane wave basis of 12.5 Ha for Si and 30 Ha for SiC. The unit cell was relaxed within the LDA approximation, yielding lattice parameters with an error smaller than 3%. The Kohn-Sham

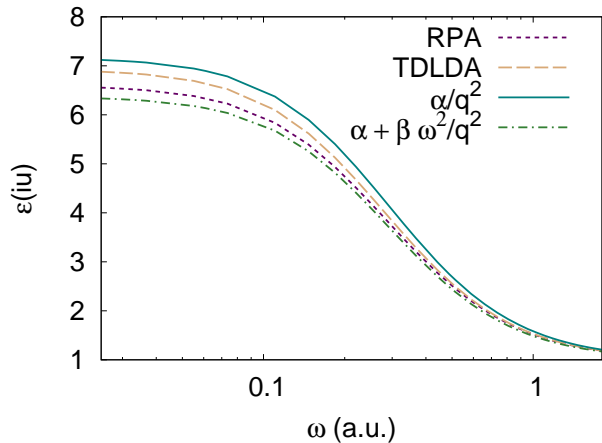


FIG. 6: (Color online) Dielectric function of SiC along the imaginary axis as a function of the frequency in a logarithmic scale. We compare results obtained within different approximations for the xc kernels.¹⁷

energies and wavefunctions yielded by ground state calculations were employed to calculate dielectric functions at imaginary frequencies using the code DP.³⁸ For the response calculations a shifted \mathbf{k} -point grid of 256 points was used both for Si and SiC. More detailed information on the numerics and convergence issues can be found in Ref. 36.

As discussed before, previous tests on the effect of different approximations for the xc potential demonstrate that the dynamical polarizability of the hydrogenated Si clusters is accurately described within the TDLDA, and therefore the C_6 coefficients are not going to change by more than 5% by using different approximations. We decide thus to focus on the effect of different models for the xc-kernel in the calculation of C_3 .

In Figs. 3 and 4 we can compare C_3 coefficients for Si clusters on a Si surface and Si clusters on a SiC surface, respectively. We present results obtained within the RPA (violet upright triangles), the TDLDA (beige inverted triangles), using the static LRC kernel (blue diamonds) and the dynamical LRC kernel (green crosses). Note that, in the case of the RPA and the TDLDA calculations, we used the Kohn-Sham band structure to build χ_0 , while the GW quasiparticle states are used when the static or dynamical LRC kernels are employed (see Refs. 36 and 37 for details). In Si and SiC the GW corrections to the bandstructures are essentially equivalent to a rigid shift of the conduction states, thus replacing KS energies with quasiparticle energies leads to a rigid shift of the absorption spectrum towards higher energies. We also plotted in Figs. 3 and 4 the values of C_3 obtained using simple models (red squares) for both the dynamical polarizability of the cluster and the dielectric function of the crystal at imaginary frequencies. We will discuss these analytical models and the quality of their results in Section IV. The peaks of C_3 as a function of the number of Si atoms occur for higher polarizable clusters. The oscillations of the

polarizabilities in turn exactly correlate with the binding energy, with largest polarizabilities corresponding to the most stable clusters.

For the interaction of Si clusters on either a Si or a SiC surface, all the approximations used for the xc kernel give curves with very similar trends and a dispersion of the values which is smaller than 10%. This finding reflects the fact that the dielectric function at imaginary frequency is a very smooth and well behaved curve, and therefore fairly simple to reproduce; it starts at the value of the static dielectric constant at $iu = 0$, and then decreases monotonically to its asymptotic limit of one (see Figs. 5 and 6).

Dielectric constants in the imaginary frequency axis can be obtained experimentally by performing a Kramers-Kronig transformation of the values obtained in the real axis,

$$\epsilon_M(iu) = 1 + \frac{2}{\pi} \int_0^\infty d\omega \frac{\omega \mathcal{J}m[\epsilon_M(\omega)]}{\omega^2 + u^2} \quad (14)$$

as long as the experimental absorption spectra has been measured on a large enough spectral range. We include in Fig. 5 the experimental curve for Si,¹⁷ for comparison. The curve calculated with the dynamical LRC approximation is exactly superposed to the experimental curve. In fact, this is the only approximation that yields a good dielectric constant, which fixes the interception with the y axis, and an overall good shape of the absorption spectrum over a large spectral range.³⁷

It is interesting to notice that the static LRC results are worse than even the RPA curve, being overestimated over the whole frequency range. In the RPA, there is a “fortuitous” compensation of errors (the error due to the too high dielectric constant is balanced by the shift of the spectral weight to lower energies due to the DFT-LDA underestimation of the absorption edge). The TDLDA curve is the one that lays further from the dynamical LRC solution at lower frequencies due to the even higher dielectric constant, but it greatly improves for $u \geq 0.1$, thanks to the same compensation of errors already observed for the RPA calculation.

The same conclusions can be obtained for SiC (see Fig. 6). In this case, we do not have access to experimental results, but it is reasonable to expect that the dynamical LRC approximation will yield the most accurate result overall. The static LRC results again shows a consistent overestimation of the dielectric function, while the the RPA curve is the closest to the dynamical LRC result.

In the light of this analysis, one can interpret the results for the C_3 coefficients. First of all, the dynamical LRC kernel is expected to work very well. Outside the limits of validity of the dynamical LRC model (large gap insulators, strongly bound excitons) only a calculation for the bulk crystal based on the solution of the BSE (or, equivalently, based on the fully ab initio Bethe-Salpeter derived kernel) can guarantee the quality of the C_3 coefficients. This implies necessarily larger computational

costs. Perhaps surprisingly, the RPA and TDLDA appear to be good approximations to evaluate C_3 , despite their well known deficiencies in the calculation of optical absorption spectra. This is not necessarily true for every system, but it is probably true provided that the calculated dielectric function at zero frequency is larger than the experimental one. In this case, in fact, we can expect the (at least partial) cancellation of error between the too high starting point of the curve $\epsilon(iu)$ and its too fast decay to one as a consequence of the shift of the spectral weight to lower energies. One should be very careful not to use the static LRC approximation for the kernel, despite the fact that it gives an absorption spectrum in overall agreement with the experiment. This is due to the fact that the van der Waals coefficients are very sensitive to the value of the dielectric constant.

IV. MODELS

Our proposed ab initio techniques are quite efficient and allow the calculation of van der Waals coefficients for systems with ~ 300 atoms, even in relatively modest computer systems. Moreover, the crystals of Si and SiC considered here contain only two atoms per unit cell and allow very fast calculations. Nevertheless, a full ab initio study of dispersion interactions of large nanostructures/biological molecules on complex surfaces can become a computationally demanding task. Therefore, it is desirable to design accurate model van der Waals potentials, based on ab-initio calculations, to be used for these calculations, where a number of atoms of the order of 1000 and even larger can be easily attained. Two problems need to be addressed: i) how to model the dynamic polarizability at imaginary frequency of the nanoobject, ii) how to model the dielectric function at imaginary frequency of the solid.

A. Model for the dielectric function

Let us start by the modelling of the semiconductor or insulator surface. We have seen that the simplest expression for the longitudinal dielectric function can be derived by applying Fermi's golden rule and assuming the case of a (nearly) homogeneous material:

$$\epsilon(\mathbf{q}, \omega) = 1 + \frac{8\pi}{q^2} \frac{1}{V} \sum_{\beta\gamma} \frac{|\langle \psi_\gamma | e^{i\mathbf{q}\cdot\mathbf{r}} | \psi_\beta \rangle|^2}{\omega_\gamma - \omega_\beta - \omega - i\eta} [f(\omega_\beta) - f(\omega_\gamma)]. \quad (15)$$

We have observed in Section III that the RPA approximation gives a rather good dielectric function at imaginary frequency thanks to a compensation of errors. It is thus reasonable to start from this simple approximation to design an analytical model. A crude approximation consists in replacing the energy differences in Eq. (15) with some average excitation energy ω_{av} . By exploiting

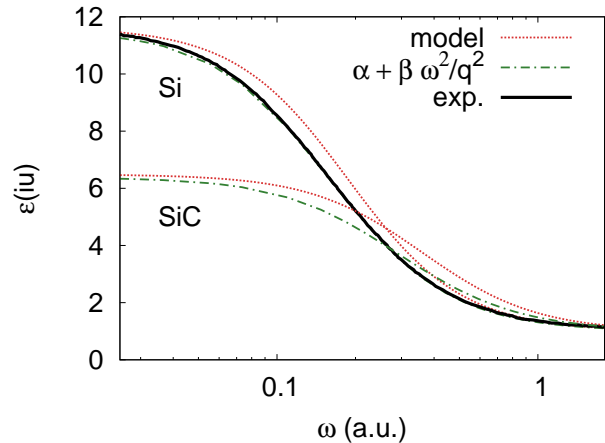


FIG. 7: (Color online) Dielectric function of Si and SiC along the imaginary axis: the model function is compared with the curve obtained using the LRC dynamical approximation for the xc kernel, which gives the best agreement with the experiment.

the sum rules and the asymptotic behavior of $\epsilon_M(\omega)$ one gets in the optical limit ($q \rightarrow 0$)⁵⁰:

$$\epsilon_M(\omega) = 1 - \frac{\omega_p^2}{\omega^2 - \omega_{av}^2 + i\eta\omega} \quad \text{with } \eta \rightarrow 0^+. \quad (16)$$

Equation (16) has the same form as the Lorentz dielectric function of bound charged carriers with frequency ω_{av} . This model predicts for the static dielectric constant

$$\epsilon_M(0) = 1 + \frac{\omega_p^2}{\omega_{av}^2}. \quad (17)$$

This equation can be used together with the value of the plasma frequency $\omega_p = 4\pi N_{el}/V$ to estimate ω_{av} . In this approximation one only needs to fix two parameters that are easily accessible from experiments, the static dielectric constant and the volume of the unit cell. At imaginary frequencies an analogous expression can be derived as a function of the same parameters:

$$\epsilon_M(iu) = 1 + \frac{\omega_p^2}{\omega_{av}^2 + u^2}. \quad (18)$$

We remind that $\epsilon_M(iu)$ is a real function. The resulting model dielectric function is plotted in Fig. 7 for both Si and SiC, together with the best theoretical curve (the one obtained using the dynamical LRC model for the xc kernel) and the experimental curve for Si. The model function is substantially worse than the calculated curves, even with respect to the RPA calculations.

B. Models for the cluster dynamical polarizabilities

For the atomic polarizabilities at imaginary frequency $\alpha(iu)$ it is convenient to use to already mentioned London

TABLE I: Values for the static polarizability $\alpha(0)$, and for the Hamaker C_6 coefficient. We show both the calculated values with (TD)DFT, as well as the values obtained using a bond polarization model (BPM) and effective medium theory (EMT), and the respective percent errors.

	$\alpha(0) \times 10^{-2}$			$C_6 \times 10^{-4}$			$\Delta C_6/C_6$ [%]	
	DFT	BPM	EMT	DFT	BPM	EMT	BPM	EMT
SiH ₄	0.349	0.422	0.337	0.0386	0.0458	0.0340	19	-11
Si ₂ H ₆	0.678	0.768	0.632	0.136	0.151	0.119	11	-9
Si ₅ H ₁₂	1.71	1.80	1.52	0.806	0.836	0.686	4	-15
Si ₈ H ₁₈	2.71	2.84	2.40	2.01	2.07	1.72	3	-14
Si ₁₀ H ₁₆	3.12	3.30	2.86	2.68	2.80	2.45	4	-9
Si ₁₇ H ₃₆	5.79	5.95	5.05	8.97	9.09	7.62	1	-15
Si ₂₀ H ₃₀	6.36	6.52	5.68	10.8	10.9	9.64	1	-10
Si ₂₂ H ₄₀	7.47	7.44	6.40	14.5	14.2	12.23	-2	-16
Si ₃₂ H ₄₂	10.0	10.2	8.96	26.5	26.7	24.0	1	-10
Si ₃₅ H ₃₆	10.7	10.8	9.59	29.9	29.8	27.49	-0.3	-8
Si ₃₈ H ₄₂	11.6	11.8	10.5	35.5	35.9	32.8	1	-8
Si ₄₇ H ₆₀	14.9	14.9	13.1	57.6	57.2	51.5	-1	-11
Si ₅₆ H ₆₆	17.6	17.6	15.5	80.0	79.3	72.0	-1	-10
Si ₆₆ H ₆₄	19.9	20.2	18.0	103	105	96.8	2	-6
Si ₇₁ H ₈₄	22.4	22.3	19.7	128	128	116	0	-10
Si ₇₄ H ₇₈	22.8	22.9	20.3	134	134	123	0	-8
Si ₈₂ H ₇₂	24.6	24.8	22.2	156	158	147	1	-6
Si ₈₆ H ₇₈	26.1	26.1	23.4	175	175	163	0	-7
Si ₈₇ H ₇₆	26.2	26.3	23.6	177	177	166	0	-6
Si ₉₉ H ₁₀₀	30.5	30.4	27.1	238	238	219	0	-8
Si ₁₀₆ H ₁₂₀	33.8	33.1	29.3	289	281	256	-3	-11
Si ₁₁₆ H ₁₀₂	34.9	35.1	31.4	314	316	295	1	-6
Si ₁₂₃ H ₁₀₀	36.8	36.9	33.2	348	349	328	0.3	-6
Si ₁₃₀ H ₉₈	38.4	38.6	34.9	381	384	363	1	-5
Si ₁₃₆ H ₁₁₀	40.7	40.7	36.6	425	426	401	0.2	-6
Si ₁₃₆ H ₁₂₀	40.9	41.1	36.9	431	434	406	1	-6
Si ₁₄₇ H ₁₀₀	43.5	43.3	39.2	484	481	459	-1	-5
Si ₁₅₉ H ₁₂₄	47.2	47.4	42.7	573	578	546	1	-5
Si ₁₆₆ H ₁₂₂	49.6	49.2	44.5	627	623	590	-1	-6
Si ₁₇₂ H ₁₂₀	50.8	50.8	45.9	661	662	630	0.2	-5

approximation, Eq. (12). In that case, two parameters for *every* cluster have to be fixed: its static polarizability $\alpha(0)$ and the energy of an effective frequency ω_1 . Of course, one does not want to define a different set of parameters for every cluster, but only two parameters for all possible clusters of a fixed species. In the case of a larger molecule or a cluster, the static polarizability can be estimated by making use of the bond polarization model (BPM)^{47,48} as suggested by Jiemchoorj *et al.*⁴⁹ In this model, the total polarizability is obtained summing over the contributions from the individual polarizable entities: the covalent bonds. In our case there are only two kinds of bonds, Si-Si and Si-H, and we can write the static polarizability as

$$\alpha_i(0) = n_i^{\text{Si-Si}} \alpha_{\text{Si-Si}} + n_i^{\text{Si-H}} \alpha_{\text{Si-H}}, \quad (19)$$

where $n_i^{\text{Si-Si}}$ and $n_i^{\text{Si-H}}$ are the number of Si-Si and Si-H bonds, respectively, of the cluster i . Here we have indicated with $\alpha_{\text{Si-Si}}$ and $\alpha_{\text{Si-H}}$ the contributions to the polarizability due to the Si-Si and the Si-H bonds, respectively. Upon substitution in the integral (2), the London model gives for a homo-molecular Hamaker constant the expression (13), and for the hetero-molecular Hamaker

constant:

$$C_6^{ij} = 3 \frac{\bar{\omega}_1^i \bar{\omega}_1^j}{2(\bar{\omega}_1^i + \bar{\omega}_1^j)} \alpha_i(0) \alpha_j(0), \quad (20)$$

where (19) gives the values of $\alpha_i(0)$. If we perform a set of ab-initio calculations of C_6^{ii} and $\alpha_i(0)$ for small-medium size clusters, we can extract ω_1^i from Eq. (13) and the parameters $\alpha_{\text{Si-Si}}$, $\alpha_{\text{Si-H}}$ by fitting the theoretical curve for the static polarizability with Eq. (19).

The small dispersion of values for ω_1^i in Fig. 2 suggests that it is possible to determine a single average frequency $\bar{\omega}_1 = 0.343$ Ha for all clusters. For the small nanocrystals with less than 10 Si atoms this approximation is not very precise, but we are interested in getting information on the interaction of larger systems, that cannot be easily studied by ab-initio techniques. The parameters $\alpha_{\text{Si-Si}}$ and $\alpha_{\text{Si-H}}$ are fixed by fitting Eq. (19) to the curve for the static polarizability calculated within the TDLDA (see Fig. 2). The outcome are the values $\alpha_{\text{Si-Si}} = 13.41$ a.u. and $\alpha_{\text{Si-H}} = 10.56$ a.u. In Table I we can verify the excellent agreement ($|\Delta\alpha(0)| \leq 1\%$ for all the clusters, excluding the smallest ones) between the static polarizabilities calculated using TDLDA and the additivity model for the

nanocrystals. The same agreement is conserved for the estimated values of C_6 : For the big clusters, the difference with the calculated values is remarkably small (see Table I).

A different approach to model the dynamic polarizability of a nanocrystal is to start from the dielectric function of the corresponding bulk crystal and apply the effective medium theory (EMT).⁵¹ This classical approach is based on the solution of Maxwell's equations with the assumption that the dielectric response of each constituent of the system is the one of the corresponding bulk. This assumption is better justified when the size of the composing objects is large. In fact, EMT completely neglects the microscopic scale details, such as atoms and bonds. In this respect it is complementary to the additive procedure. However, it handles correctly the boundary conditions for the Maxwell's equations at the interfaces, which give very important contributions to the dielectric response through the crystal local field effects. Our clusters can be considered as a sphere of Si in vacuum with a filling factor f that goes to zero. The Maxwell-Garnett expression⁵¹ yields in this specific case:

$$\Im\{\alpha(\omega)\} = \frac{-9V_s}{4\pi} \Im\left\{\frac{1}{\epsilon_M^{\text{Si}}(\omega) + 2}\right\}, \quad (21)$$

where ϵ_M^{Si} is the complex dielectric function of bulk silicon, and where V_s is the volume of the spherical cluster. By applying the analogous of the Laplace transformation (14) to the dynamical polarizability at real frequencies and using once again the single-oscillator model (16) for the dielectric function of bulk Si, we obtain for the dynamical polarizability at imaginary frequencies:

$$\alpha(iu) = \frac{V_s}{4\pi} \frac{\omega_p^2}{u^2 + \omega_{\text{av}}^2 + \omega_p^2/3}, \quad (22)$$

This expression can be rewritten in the same form as the London model by imposing:

$$\alpha(0) = \frac{V_s}{4\pi} \frac{\omega_p^2}{\omega_{\text{av}}^2 + \omega_p^2/3} \quad (23)$$

and

$$\omega_1 = \sqrt{\omega_{\text{av}}^2 + \omega_p^2/3}. \quad (24)$$

With respect to the model for the dielectric function of the crystal we have here an extra parameter to be estimated: the volume of the spherical cluster. In the limit of a very large cluster, we can assume that the volume per Si atom is the same as in the bulk crystal. To obtain better results for small-medium sized clusters it is necessary to include the contribution to the volume due to the hydrogen atoms at the surface (considering a Si-H bond distance of about 1.5Å, we can assume a volume of about 11.4 a.u. per hydrogen atom). The value of ω_1 is 0.4Ha, which is 20% larger than ω_1 evaluated in the

BPM. The values of $\alpha(0)$, on the other hand, are systematically smaller than their counterparts in the BPM. As a result, C_6 coefficients are underestimated by about 5% for the larger clusters and up to 10-15% for the smaller ones.

The non-trivial advantage of this second approach is the fact that no ab-initio calculation needs to be performed to fit $\alpha(0)$ and ω_1 .

C. Modelled C_3 coefficients

Finally, we calculated the C_3 coefficients both for Si nanocrystals on Si surfaces and on SiC surfaces combining the single-oscillator model for the surface the the bond polarization model for the nanocrystal. The curves obtained are plotted in Figs. 3 and 4 where they can be compared with the results of the ab-initio calculations. The model calculations are rigidly shifted to higher values by about 5% for Si and 7% for SiC (when compared with the dynamical LRC model). Curiously, they almost overlap with the results obtained using the LRC xc kernel for the determination of the dielectric function. This can be understood by inspecting Fig. 7: the error is likely to be entirely due to the insufficiently accurate description of the dielectric function of the bulk material.

V. CONCLUSIONS

We have demonstrated how the leading terms of the van der Waals forces acting between nanostructures, and between nanostructures and non-metallic surfaces, can be accurately and inexpensively computed from first principles. The key ingredients can be reliably obtained with state-of-the-art theoretical schemes and computational procedures. The dynamical polarizabilities of large nanostructures at imaginary frequencies, for example, can be safely computed with the Sternheimer reformulation of time-dependent density-functional theory. Regarding the other key ingredient necessary to obtain the cluster-surface interaction, the macroscopic dielectric constant, it can also be computed by making use of TDDFT. In this case, special care has to be taken with the choice of the xc kernel. We have found that a particularly simple and reliable scheme is to make use of the dynamical "long-range contribution" (LRC) kernel.³⁷ However, if the bulk to be studied lies outside the limits of validity of the dynamical LRC model (large gap insulators, systems with strongly bound excitons), one probably has to resort to the full solution of the Bethe-Salpeter equation (or, equivalently, to a TDDFT calculation based on a kernel derived from the Bethe-Salpeter equation).³⁴ This necessarily implies larger computational costs.

We also suggest some simplified models that should supply reasonable estimates for the van der Waals coefficients, for those cases in which first principle calculations are out of range. We have found that modelling

the bulk dielectric function can lead to a substantial error ($\sim 10\%$). However, using a bond polarization model or the effective medium theory for the nanostructure dynamical polarizability, yields very precise results, especially for large systems. This opens the way to the simulation of the van der Waals interaction for large nanocrystals.

Acknowledgments

All calculations were performed at the Laboratório de Computação Avançada of the University of Coimbra. The authors were partially supported by the EC Net-

work of Excellence NANOQUANTA (NMP4-CT-2004-500198). S. Botti acknowledges financial support from French ANR (JC0546741). A. Castro acknowledges financial support from the Deutsche Forschungsgemeinschaft within the SFB 658. X. Andrade acknowledge partial support from the EU Programme Marie Curie Host Fellowship (HPMT-CT-2001-00368). M.A.L. Marques acknowledges partial support by the Portuguese FCT through the project PTDC/FIS/73578/2006. X. Andrade and A. Rubio acknowledge financial support from the Spanish Ministry of Education (Grant No. FIS2007-65702-C02-01) and Grupos Consolidados UPV/EHU of the Basque Country Government (2007).

-
- * Electronic address: silvana.botti@polytechnique.edu
- ¹ J. Israelachvili, *Intermolecular and Surface Forces* (Academic Press, San Diego, 1992); J. Mahanty and B. W. Ninham, *Dispersion Forces* (Academic Press, New York, 1976).
 - ² J. D. van der Waals, Ph.D. thesis, University of Leiden, 1873; translated to English by R. Threlfall and J. F. Adair, in *Physical Memoirs, Selected and Translated from Foreign Sources*, 1 (Physical Society, London, 1890), 333.
 - ³ Y. Tian, N. Pesika, H. B. Zeng, K. Rosenberg, B. X. Zhao, P. McGuiggan, K. Autumn, J. Israelachvili, Proc. Natl. Acad. Sci. USA **103**, 19320 (2006).
 - ⁴ G. Binnig, C. F. Quate and Ch. Gerber, Phys. Rev. Lett. **56**, 930 (1986).
 - ⁵ F. Shimizu, Phys. Rev. Lett. **86**, 987 (2001); V. Druzhinina and M. DeKieviet, Phys. Rev. Lett. **91**, 193202 (2003).
 - ⁶ D. M. Harber, J. M. McGuirk, J. M. Obrecht and E. A. Cornell, J. Low. Temp. Phys. **133**, 229 (2003); A. E. Leanhardt, Y. Shin, A. P. Chikkatur, D. Kielpinski, W. Ketterle and D. E. Pritchard, Phys. Rev. Lett. **90**, 100404 (2003); Y. J. Lin, I. Teper, C. Chin and V. Vuletić, Phys. Rev. Lett. **92**, 050404 (2004).
 - ⁷ H. B. Chan, V. A. Aksyuk, R. N. Kleiman, D. J. Bishop and F. Capasso, Phys. Rev. Lett. **87**, 211801 (2001); H. B. Chan, V. A. Aksyuk, R. N. Kleiman, D. J. Bishop, and Federico Capasso, Science **291**, 1941 (2001).
 - ⁸ J. F. Dobson, A. White, A. Rubio, Phys. Rev. Lett. **96**, 073201 (2006).
 - ⁹ H. C. Hamaker, Physica (Amsterdam) **4**, 1058 (1937).
 - ¹⁰ B. Jeziorski, R. Moszynski and K. Szalewicz, Chem. Rev. **94**, 1887 (1994).
 - ¹¹ J. E. Lennard-Jones, Trans. Faraday Soc. **28**, 333 (1932).
 - ¹² H. B. G. Casimir and D. Polder, Nature **158**, 787 (1946); Phys. Rev. **73**, 360 (1948).
 - ¹³ E. M. Lifshitz, Zh. Eksp. Teor. Fiz. **29**, 94 (1956) [Sov. Phys. JETP **2** 73, (1956)].
 - ¹⁴ E. Zaremba and W. Kohn, Phys. Rev. B **13**, 2270 (1976).
 - ¹⁵ V. Sandoghdar, C. I. Sukenik, E. A. Hinds and S. Haroche, Phys. Rev. Lett. **68**, 3432 (1992).
 - ¹⁶ M. Fichet *et al.*, Eur. Phys. Lett. **77**, 54001 (2007), and references therein.
 - ¹⁷ A. O. Caride, G. L. Klimchitskaya, V. M. Mostepanenko, and S. I. Zhanette, Phys. Rev. A **71**, 042901 (2005).
 - ¹⁸ S. H. Patil, K. T. Tang and J. P. Toennies, J. Chem. Phys. **116**, 8118 (2002); E. Hult and A. Kiejna, Surf. Sci. **383**, (1997); A. Liebsch, Phys. Rev. B **35**, 9030 (1987); G. Vidal and M. W. Cole, Surf. Sci. **110**, 10 (1981).
 - ¹⁹ Y. Andersson, D. C. Langreth, and B. I. Lundqvist, Phys. Rev. Lett. **76**, 102 (1996); E. Hult, Y. Andersson, B. I. Lundqvist and D. C. Langreth, Phys. Rev. Lett. **77**, 2029 (1996); E. Hult, H. Rydberg, B. I. Lundqvist and D. C. Langreth, Phys. Rev. B **59**, 4708 (1999); Y. Andersson and H. Rydberg, Phys. Scripta **60**, 211 (1999).
 - ²⁰ M. A. L. Marques, C. Ullrich, F. Nogueira, A. Rubio and E.K.U. Gross (editors), *Time-Dependent Density-Functional Theory*, Lecture Notes in Physics 706, Springer Verlag, Berlin (2006).
 - ²¹ S. J. A. van Gisbergen, J. G. Snijders, and E. J. Baerends, J. Chem. Phys. **103**, 9347 (1995).
 - ²² M. A. L. Marques, A. Castro, G. Mallocci, G. Mulas, and S. Botti, J. Chem. Phys. **127**, 014107 (2007).
 - ²³ P. Norman, D. M. Bishop, H. J. A. Jensen and J. Oddershede, J. Chem. Phys. **115**, 10323 (2001); Norman, A. Jiemchoorj and B. E. Semelius, J. Chem. Phys. **118**, 9167 (2003); A. Jiemchoorj, P. Norman and B. E. Semelius, J. Chem. Phys. **123**, 124312 (2005); A. Jiemchoorj, P. Norman and B. E. Semelius, J. Chem. Phys. **125**, 124306 (2006).
 - ²⁴ A. Banerjee and M. K. Harbola, J. Chem. Phys. **117**, 7845 (2002); A. Banerjee and M. K. Harbola, PRAMANA J. Phys. **66**, 423 (2006); A. Banerjee and M. K. Harbola, arXiv:0801.1424v1 (2008).
 - ²⁵ R. Sternheimer, Phys. Rev. **84**, 244 (1951).
 - ²⁶ S. Baroni, S. de Gironcoli, A. D. Corso, and P. Gianozzi, Rev. Mod. Phys. **73**, 515 (2001), and references therein.
 - ²⁷ G. Senatore and K. R. Subbaswamy, Phys. Rev. A **35**, 2440 (1987); S. P. Karna and M. Dupuis, Chem. Phys. Lett. **171**, 201 (1990); S. J. A. van Gisbergen, J. G. Snijders, and E. J. Baerends, Phys. Rev. Lett. **78**, 3097 (1997); J. I. Iwata, K. Yabana, and G. F. Bertsch, J. Chem. Phys. **115**, 8773 (2001); B. Walker, A. M. Saitta, R. Gebauer, and S. Baroni, Phys. Rev. Lett. **96**, 113001 (2006).
 - ²⁸ M. A. L. Marques, A. Castro, G. F. Bertsch and A. Rubio, Comp. Phys. Comm. **151**, 60 (2003); A. Castro, M. A. L. Marques, H. Appel, M. Oliveira, C. Rozzi, X. Andrade, F. Lorenzen, E. K. U. Gross and A. Rubio, phys. stat. sol. (b) **243**, 2465 (2006).
 - ²⁹ X. Andrade, S. Botti, M. A. L. Marques, and A. Rubio, J.

- Chem. Phys. **126**, 184106 (2007).
- ³⁰ L. Hedin, Phys. Scripta **21**, 477 (1980).
- ³¹ G. Onida, A. Rubio and L. Reining, Rev. Mod. Phys. **74**, 601 (2002).
- ³² R. Del Sole and R. Girlanda, Phys. Rev. B **48**, 11789 (1993).
- ³³ W. Hanke, Adv. Phys. **27**, 287 (1978).
- ³⁴ S. Botti, A. Schindlmayr, R. Del Sole, and L. Reining, Rep. Prog. Phys. **70**, 357 (2007), and references therein.
- ³⁵ L. Reining, V. Olevano, A. Rubio, G. Onida, Phys. Rev. Lett. **88**, 066404 (2002).
- ³⁶ S. Botti, F. Sottile, N. Vast, V. Olevano, L. Reining, H. C. Weissker, A. Rubio, G. Onida, R. Del Sole, R. W. Godby, Phys. Rev. B **69**, 155112 (2004).
- ³⁷ S. Botti, A. Fourreau, F. Nguyen, Y. O. Renault, F. Sottile and L. Reining, Phys. Rev. B **72**, 125203 (2005).
- ³⁸ V. Olevano, L. Reining and F. Sottile, <http://theory.polytechnique.fr/codes/dp/>.
- ³⁹ J. M. Soler, E. Artacho, J. D. Gale, A. García, J. Junquera, P. Ordejón, and D. Sánchez-Portal, J. Phys.: Condens. Matter **14**, 2745 (2002).
- ⁴⁰ J. P. Perdew, K. Burke, and M. Ernzerhof, Phys. Rev. Lett. **77**, 3865 (1996).
- ⁴¹ N. Troullier and J. L. Martins, Phys. Rev. B **43**, 1993 (1991).
- ⁴² J. P. Perdew and A. Zunger, Phys. Rev. B **23**, 5048 (1981).
- ⁴³ I. Vasiliev, S. Ogut, and J. R. Chelikowsky, Phys. Rev. Lett. **86**, 1813 (2001); M. C. Tjorheim, L. Kronik, and James R. Chelikowsky, Phys. Rev. B **65**, 033311 (2001). S. Botti and M. A. L. Marques, Phys. Rev. B **75**, 035311 (2007).
- ⁴⁴ M. A. L. Marques, A. Castro and A. Rubio, J. Chem. Phys. **115**, 3006 (2001).
- ⁴⁵ X. Gonze *et al*, Comp. Mat. Sci. **25**, 478 (2002); X. Gonze *et al*, Zeit. Kristallogr. **220**, 558 (2005).
- ⁴⁶ D. R. Hamann, M. Schlüter and C. Chiang, Phys. Rev. Lett. **43**, 1494 (1979).
- ⁴⁷ M. V. Wolkenstein, C. R. Acad. Sci. URSS **30**, 791 (1941).
- ⁴⁸ *Light Scattering in Solids II*, edited by M. Cardona and G. Güntherodt (Springer-Verlag, Berlin, 1982).
- ⁴⁹ A. Jiemchoorj, B. E. Sernelius, and P. Norman, Phys. Rev. A **69**, 044701 (2004).
- ⁵⁰ G. Grosso and G. Pastori Parravicini, *Solid State Physics*, Elsevier Academic Press, London (2000).
- ⁵¹ J. C. Maxwell-Garnett, Philos. Trans. R. Soc. **203**, 385 (1904); D. M. Wood and N. W. Ashcroft, Philos. Mag. **35**, 269 (1977).